Title

A novel technique for accurate electrode placement over cortical targets for transcranial electrical stimulation (tES) clinical trials.

Journal

Journal of Neural Engineering, 18(5)

Authors

Jog, Mayank
Anderson, Cole
Kim, Elizabeth
et al.

Publication Date

2021-10-11

DOI

10.1088/1741-2552/ac297d

Peer reviewed

HHS Public Access

Author manuscript

J Neural Eng. Author manuscript; available in PMC 2022 October 11.

Published in final edited form as:

J Neural Eng. ; 18(5): . doi:10.1088/1741-2552/ac297d.

A novel technique for accurate electrode placement over cortical targets for transcranial electrical stimulation (tES) clinical trials

Mayank Jog[a], **Cole Anderson**[a], **Elizabeth Kim**[a], **Avery Garrett**[a], **Antoni Kubicki**[a], **Sara Gonzalez**[a], **Kay Jann**[b], **Marco Iacoboni**[a], **Roger Woods**[a], **Danny JJ Wang**[b], **Katherine L. Narr**[a,*]

[a]Department of Neurology, University of California Los Angeles, Los Angeles, California, United States.

[b]Stevens Neuroimaging and Informatics Institute, University of Southern California, Los Angeles, California, United States.

Abstract

Objective: We present an easy-to-implement technique for accurate electrode placement over repeated transcranial electrical stimulation (tES) sessions across participants and time. tES is an emerging, non-invasive neuromodulation technique that delivers electrical stimulation using scalp electrodes.

Approach: The tES electrode placement technique was developed during an exploratory clinical trial aimed at targeting a specific MNI-atlas cortical coordinate in N=59 depressed participants (32F, mean age: 31.1 ± 8.3 SD). Each participant completed 12 sessions of active or sham stimulation, administered using high-definition (HD) or conventional sized electrode montages placed according to the proposed technique. Neuronavigation data measuring the distances between the identified and the intended stimulation site, simulations, and cerebral blood flow (CBF) data at baseline and post-treatment were acquired to evaluate the targeting characteristics of the proposed technique.

Main results: Neuronavigation measurements indicate accurate electrode placement to within 1cm of the stimulation target on average across repeated sessions. Simulations predict that these placement characteristics result in minimal electric field differences at the stimulation target (>0.90 correlation, and <10% change in the modal electric field and targeted volume). Additionally, significant changes in %CBF (relative to baseline) under the stimulation target in the active stimulation group relative to sham confirmed that the proposed placement technique introduces minimal bias in the spatial location of the cortical coordinate ultimately targeted. Finally, we show proof of concept that the proposed technique provides similar accuracy of electrode placement at other cortical targets.

Significance: For voxel-level cortical targets, existing techniques based on cranial landmarks are suboptimal. Our results show that the proposed electrode placement approach provides high

*Corresponding author: narr@ucla.edu.

Declaration of conflicts of interest:
The authors confirm that there are no known conflicts of interest associated with this publication.

consistency for the accurate targeting of such specific cortical regions. Overall, the proposed technique now enables the accurate targeting of locations not accessible with the existing 10–20 system such as scalp-projections of clinically-relevant cortical coordinates identified by brain mapping studies.

Clinical trial ID: NCT03556124

Keywords

Transcranial Electrical Stimulation (tES); transcranial direct current stimulation (tDCS); electrode placement; neuromodulation; neuronavigation; cortical targeting

Introduction:

Transcranial electrical stimulation (tES) is an emerging non-invasive neuromodulation technique that uses scalp electrodes to modulate cortical excitability. Following the demonstration of motor evoked potential (MEP) changes using direct current stimulation (1), tES has been reported to improve symptoms in neurologic and psychiatric disorders, as well enhance cognition (2–5). A typical tES montage utilizes large (~25cm^2) sponge electrodes placed over the scalp to deliver milliampere electric currents of a particular type, including direct, alternating as well as random noise stimulation (6, 7). Simulations have shown the electric current to be diffuse, in part due to the large size of the electrodes (8, 9), yet capable of modulating cortical excitability (1, 10).

Recently, montages with focal stimulation have been shown to be more efficient than conventional montages, as measured by MEP changes in the motor cortex after direct current stimulation (11). Focal stimulation is made possible by employing multiple small electrodes in a special setup such as with high-definition transcranial direct current stimulation HD-tDCS (12, 13). Simulations have predicted these focal montages to be more sensitive to inter-individual differences in anatomy than conventional setups (14, 15), a challenge that could be accounted for by personalizing tES montages to individual subjects (16). However, the overall increased sensitivity of focal montages to local anatomical parameters means that as more efficient focal montages utilizing multiple small electrodes are developed (17, 18), ensuring accurate placement of electrodes becomes an increasingly important concern. Inaccurate electrode placement could potentially reduce the efficacy of tES (19–21) and also introduce inter-subject variability in response to treatment, an issue that has recently been highlighted in the published literature (22, 23).

The challenge of accurate electrode placement is especially important in the case of clinical trials, where treatment effects are evaluated after multiple tES sessions in the same participant (24, 25). Typically, electrode placement in tES is carried out using the 10–20 EEG system electrode placement technique (26, 27). However, the cranio-cortical relationship in the 10–20 system is not precise, and variations in the order of 8mm have been reported for cortical projections of the same 10–20 coordinate across individuals (28, 29). Coupled with operator inaccuracies (as shown for C3 and C4 coordinates in (30)), the accumulating inaccuracy in electrode placement may affect which cortical regions are ultimately targeted, especially in the case of spatially focal montages like HD.

A better choice for stimulation sites could be scalp projections of cortical targets identified by brain mapping studies. However, it is not straightforward to extend the 10–20 system (which is based on cranial landmarks and distances) to accurately identify projections of specific cortical targets over the scalp within and across participants. An alternative is to use neuronavigation systems (31), which utilize infrared cameras and associated software to map positions on the participant's scalp to a reference (*e.g.*, a structural MRI image of the same participant). Using a neuronavigation approach for electrode placement during every visit for every participant would be ideal, but doing so would be quite resource intensive in practice.

In this study, we present an easy-to-implement technique to allow for stimulation of homologous cortical regions across independent stimulation sessions. The proposed technique extends accurate electrode placement to include locations not accessible with the 10–20 system (e.g., scalp-projections of clinically-relevant cortical targets), and was developed for an ongoing clinical trial (NCT03556124) where targeting of an *a-priori* selected cortical coordinate location by 12 sessions of transcranial direct current stimulation (tDCS) had been hypothesized to improve depressive symptoms (32, 33). Here, the accuracy of placement was quantified using state-of-the-art frameless stereotaxic neuronavigation equipment, and this data was used in simulations to show that the measured variability in electrode placement generates minimal changes in the electric field distribution at the stimulation target. Additionally, cerebral blood flow (CBF) measurements were utilized to measure the location of stimulation induced changes in CBF and investigate any potential biases introduced by the proposed electrode placement technique in targeting. Finally, we provide proof of concept that the proposed technique is capable of providing a similar accuracy of electrode placement at targets over the entire scalp.

Methods:

1. Participants and experimental design:

Subjects included N=59 participants with major depression (32F, mean age: 31.1 ± 8.3 SD) who completed a clinical trial designed to investigate how blood flow and neurophysiological markers of neuronal activity (e.g. Arterial Spin Labeling measured cerebral blood flow (CBF), and the blood oxygenation level dependent (BOLD)-fMRI) differ in the brain following repeated tDCS treatment (32, 33). Upon enrollment, participants were randomly assigned into one of four groups: high-definition (i.e. HD)-tDCS or Conventional-tDCS (montage) x Active or Sham stimulation, with N=20, 19, 10, and 10 participants in the Active-HD, Active-Conventional, Sham-HD and Sham-conventional groups respectively. Post-randomization, participants underwent 12 sessions of 20 minutes x 2 mA of tDCS over 12 consecutive working days. Participants as well as study staff were blinded to the type of stimulation (Active/Sham), and were polled at the end of each participant's treatment session to verify integrity of blinding, evaluated by comparing differences in guesses of active/sham stimulation between groups using a χ^2 test.

The stimulation target was selected to be located at $x=-46, y=44, z=38$ in MNI coordinates, based on prior studies in major depression (34, 35). As shown in Fig 1.A, a 4×1 electrode arrangement with 2×2 cm sized electrodes was used for the HD montage, with the anode placed at the stimulation target and the cathode electrodes positioned 5 cm away from the

central anode and equidistant from the two adjacent cathode electrodes. For the conventional montage (hereafter referred to as “Conv”), tDCS was delivered using 5×7 cm sponge electrodes with the anode positioned at the target and cathode placed over *x=56, y=30, z=−1* (MNI coordinates), near the F8 location (10–20 EEG system) that overlies the inferior frontal gyrus (36). All participants provided informed consent following approval of study procedures by the Institutional Review Board (IRB) at the University of California Los Angeles.

MRI structural data to guide the electrode placement was acquired prior to tDCS treatment sessions at visit 0 (Fig. 1B). The structural data was acquired using a T1 MPRAGE scan on a 3T Siemens PRISMA scanner with the Human Connectome Project Lifespan sequence parameters (37). Additional MRI scans to evaluate target engagement and neurophysiological changes with treatment were also acquired. Of these, data from a 3D GRASE pseudo continuous arterial spin labeling (pCASL) sequence was used to measure cerebral blood flow (CBF) (38). Sequence parameters for the pCASL sequence were: TR/TE=4000/25ms, 96×96 matrix, 2.5×2.5×2.5mm^3, 48 slices, labeling duration=1.5sec, post-labeling delay = 1.8s; N = 2 back-to-back scans (data was averaged post CBF-quantification). In addition to the imaging data, the Brainsight neuronavigation system (Brainsight (39)), comprising an infrared camera and associated software was used to track the position of the stimulating electrode, as described below.

2. Electrode placement:

Each participant was fitted with a cap (EASYcap (40)) on their first visit. As shown in Fig 2.A, a cap size that the participant found comfortable was chosen and secured with a chin strap. The strap was then marked with a pen, so the cap could be secured with the same tension for all subsequent stimulation sessions. Next, the nasion to inion distance was measured and recorded. The cap, pre-marked by the vendor with 10–20 EEG coordinates, was adjusted such that the midpoint of the line joining Fp1 and Fp2 was 10% of the nasion-to-inion distance (Fig. 2.B). Following this, the cap was adjusted such that the T7 and T8 reference points were at identical distances from the left (L) and right (R) tragus (Fig. 2.C). Finally, the cap was secured by taping it down over the participant’s upper cheeks and between the eyebrows. The nasion to Fp1/Fp2, and L/R tragus to T7/T8 distances were recorded, and for all subsequent sessions with the same participant, the EEG cap was placed to match these distances to within 0.2 cm. Note that the precise correspondence of the reference points to the actual locations of T7, T8 etc. is not important; what is crucial is to ensure that the distances of these reference points from anatomical landmarks are within the 0.2 cm tolerance for correct cap-placement. The 0.2 cm tolerance was chosen since it is 2 times the minimum measurable distance on a standard measuring tape.

Next, the stimulation target was marked on the cap using a state-of-the-art frameless stereotaxic neuronavigation system (Brainsight, (39)). Here, the participant’s T1-structural image (acquired during visit 0) was first registered to the participant fitted with the cap as follows: 1. Fiducials mounted on an external probe were moved to each of three reference points (the nasion and the left and right tragus). 2. When in position, the Brainsight infrared camera and associated software was used to register the real-world positions of these

reference points to their respective counterparts in the digital MRI image. Once this real-world to digital MRI image mapping was established, the neuronavigation system was used to locate and mark the stimulation target on the participant's cap. This was done by moving the fiducial-fitted external probe to the location corresponding to the stimulation target in the digital MRI image (now being mapped to real-world space through the neuronavigation registration described in 1. and 2. above). The location of the stimulation-target in the digital MRI image was calculated by transforming the MNI coordinates of the stimulation target to each individual participant's T1 image space (implemented using SPM12, inverse normalization, (41)), followed by the shortest distance projection of the coordinates from the cortical location onto the scalp. Note that a precise localization of the stimulation target using neuronavigation is needed only at the initial (pretreatment) visit. For the 11 subsequent tDCS sessions, electrode placement was performed by staff by first placing the cap using the procedure described above, followed by using the now-marked cap to identify the stimulation site on the scalp.

3. Accuracy of electrode placement:

The accuracy of electrode placement was assessed using neuronavigation. During each treatment visit, the electrode placement site was identified using the cap placement procedure described in section 2. At the mid-trial visit (visit #6), Brainsight neuronavigation was used to record the displacement between the anode electrode's site (identified using the previous cap placement step) and the intended scalp target. Due to scheduling constraints, this data could only be acquired for 48 of the enrolled participants (N=23 and 25 in the HD and conventional groups respectively). Here, the mean, standard deviation and maximum displacements were calculated for analysis.

4. Simulations of electrode displacements:

Next, simulations were utilized to investigate the impact of the experimentally observed electrode displacements on electric fields at the stimulation target. Specifically, a 5-compartment model of the MNI152 head (available with FSL (42)) was generated using SIMNIBS (43). Using the default tissue conductivities provided in SIMNIBS (from (44, 45)), simulations of the electric fields were generated for: (1) 0mm displacement (i.e. the ideal case), (2) the experimentally measured average electrode displacements (described in section 3 above), and (3) electrodes displaced by 1 and 2cm (i.e. half, and full length of the smallest electrode dimension (Fig 1)).

A spherical region of interest (ROI) of radius 1cm and centered at the stimulation target was constructed for analysis. The ROI was masked to include only gray and white matter voxels, with the gray and white matter masks being generated from segmentation of the MNI152 image (using SPM12 (41)). Electric field magnitudes within the ROI were extracted and compared to the zero-displacement case using the following metrics : (a) Pearson correlation coefficient, (b) %change in the modal electric field, and (c) %change in the "targeted volume". The targeted volume is defined as the percentage of voxels in the ROI where the electric field is greater than 50% of the modal electric field of the zero-displacement case. While (a) tracks changes in the spatial distribution of the electric field, (b) measures changes in the average electric field in the ROI, and (c) tracks changes in the total brain

volume being targeted. For each displacement value, models were generated wherein the anodal electrode was displaced in the anterior, posterior, and lateral directions over the scalp. The calculated metrics were averaged over the simulated models for each displacement value and are reported in the results section. Note that the mode was selected over the mean, since the electric field distribution within the ROI was observed to be heavy-tailed. The mode was calculated from binned data, with the histogram bin-widths following the Freedman-Diaconis criterion, which is recommended for heavy-tailed distributions (46, 47). Finally, an identical analysis on simulated electric fields normal to the cortical surface (calculated using SIMNIBS (43)) was also performed.

5. Cerebral blood flow changes at the stimulation target:

PCASL data from two participants was excluded because of MRI reconstruction errors. The remaining data from 57 participants was motion corrected using SPM12 (41), and used to quantify CBF using in-house preprocessing streams (48). The calculated CBF maps were normalized to the MNI space using SPM12, masked using a gray matter mask (SPM12 TPM mask, thresholded at gray matter probability > 0.2) and smoothed using a 7.5mm (3 voxel wide) kernel. Following this, %ch-CBF maps were calculated as $(CBF_{post\text{-}treatment}-CBF_{baseline})/CBF_{baseline}$ *100, the percentage metric being used to control for potential baseline differences in CBF between participants. Finally, a 2 sample t-test was used to investigate differences in %ch-CBF between the active-stimulation and sham groups at the left DLPFC stimulation-target, with the expectation of observing significant changes in CBF, consistent with (49, 50). Here, the left DLPFC was defined using an anatomical ROI from the Sallet (51) atlas. To determine the location of the peak significant voxel to compare with the intended stimulation target, post-hoc voxel-wise t-tests were performed in the same region and thresholded at $p < 0.05$.

6. Other brain targets:

Finally, we investigated the accuracy of the developed technique for electrode placement over the rest of the scalp. To provide proof of concept, data was acquired from a small sample of 4 participants x 2 raters. Early piloting had indicated that using the left tragus to C3, the right tragus to C4, and left/right tragus to Cz distances instead of left tragus to T7 and right tragus to T8 in cap placement provided slightly better accuracy in electrode placement. Consequently, cap placement was performed with these reference points instead of T7 and T8, with all other steps identical to those described in section 2. Cortical coordinates of projections of F2, Fz, F4, F8, Cz, C4, T4, Pz, P4, T6, and O2 in the MNI space (reported in (28)) were chosen as brain-targets. The rationale for choosing these locations was to ensure reasonable coverage of the full scalp. The scalp positions of these targets for individual participants were calculated as described in section 2, and marked on the cap using the Brainsight neuronavigation system. Next, the cap placement procedure was repeated, and distances between recorded coordinates and the intended scalp targets were recorded using the neuronavigation system. These measurements were used to calculate the mean, standard deviation and maximum displacement values.

Results:

Table 1 shows the distances between the anodal electrode's site and the stimulation target, measured using neuronavigation. Overall, an average electrode displacement of 7.0 ± 2.8 mm was observed, with a maximum displacement of 13 mm. No significant differences in displacements were observed between the HD and Conv groups ($p = 0.44$, two sample t-test), with the HD group showing a mean displacement of 6.7 ± 2.7 mm, and the Conv group showing a mean displacement of 7.3 ± 3.0 mm.

Fig 3 shows the distribution of the electric field in the 1cm ROI at the stimulation target, simulated for the ideal, zero-displacement case. As can be seen, the field distribution is heavy-tailed, providing motivation for the use of the modal electric field as a summary statistic (rather than the mean). Overall, simulations predicted a modal electric field (in V/m) and targeted volume (in %) of: (a) (0.11, 100%), (0.15, 100%) calculated with the electric field strength for the conventional and HD montages respectively, and (b) (0.09, 62.03%), (0.14, 58.70%) calculated with the electric field normal to the cortical surface for the conventional and HD montages respectively. Table 2.A shows the changes in electric field strength with different electrode displacement values. With 7mm displacement (i.e. the average displacement measured with the electrode placement technique, see Table 1), a correlation of 0.99, 3.49% change in the modal electric field strength and no measurable change in the targeted volume was observed for the conventional montage. A slightly lower correlation of 0.91, −2.13% change in the modal electric field, and no measurable change in the targeted volume was observed with the HD montage.

Two additional scenarios were simulated in order to understand the impact of electrode displacements on the electric field distribution. Here, the electrodes were displaced by 1 and 2 cm (i.e. half and full-size respectively, of the smallest electrode's dimensions, see Fig 1). Overall, average correlations were observed to be > 0.80, with < 15% change in the modal electric field and < 5% change in the targeted volume, with the exception of the 2cm displacement case for the HD montage (where an average correlation of 0.58 was observed). Similar results were observed with electric fields normal to the cortical surface (Table 2.B), with correlations > 0.80, <15% change in the modal electric field, and < 5% change in the targeted volume, with the exception, as before, of the 2cm displacement case for the HD montage. Here, a correlation of 0.74 was observed, along with large scale changes in the modal electric field and targeted volume (−45.37%, and −30.93% respectively). Note that the metrics shown in Table 2 were calculated as averages over simulations where the electrode was displaced in the anterior, posterior, and lateral directions, for a particular displacement distance (as described in methods). The unaveraged directional metrics are shown in Supplementary S1, and show the same pattern.

Significant increases in %ch-CBF between active-stimulation and sham were observed in the left DLPFC region (Fig 4). Posthoc voxelwise t-tests revealed a significant ($p < 0.05$) cluster within this region, with the peak significant voxel located at $x=-27, y=42, z=19.5$ mm (MNI co-ordinates). For comparison, the cortical stimulation target is shown with a white arrow. No significant differences in %ch-CBF between the HD and conventional active-stimulation montages were observed for the same region ($p=0.29$).

Finally, Table 3 shows the average and maximum displacements measured for targets over the rest of the scalp in a test sample. Overall, the electrodes were displaced by 4.28mm ± 2.29 mm on average, with a maximum displacement of 12.79 mm, which is slightly better than the accuracy observed in the previous cohort (=7.0 ± 2.8 mm, see Table 1).

No significant differences were observed with regard to active/sham guesses between the active and sham stimulation groups, verifying integrity of blinding (Participants: χ^2 =1.54, p=0.46; Staff: χ^2 =0.045, p=0.97).

Discussion:

In this work, we describe and validate a technique that ensures accurate electrode placement (to < 1cm on average) at *x=−46mm, y=44mm, z=38mm* (MNI), a target of interest for neuromodulation in major depression (32, 34). Additionally, we demonstrate that this technique provides a similar accuracy for electrode placement at other targets over the scalp in a test sample. The key contribution of this work is that it provides an easy-to-implement method to position electrodes accurately over repeated tES sessions across different days and participants. This accurate positioning is not limited to 10–20 EEG coordinates, making it possible to target clinically relevant cortical coordinates (as was the case in our clinical trial), or spatially specific nodes of a resting-state (52), or task network-of-interest (53).

Most tES studies to date place the tES stimulating electrode using the 10–20 EEG system. The 10–20 system utilizes cranial landmarks, and placement is performed after identifying the 10–20 coordinate nearest to the cortical target of interest (6, 24). This approximation introduces a bias in the position of the electrode compared to the scalp projection of the cortical target. Critically, this approach also introduces variability on the order of 8mm on average across individuals, since the cranio-cortical relationship in the 10–20 system is not precise (28). Added to this is the variability introduced by operator inaccuracies, for instance, ~5mm as shown for C3 and C4 locations in (30), which are further amplified for locations derived from C3 and C4 in the 10–20 system. Overall, these accumulating inaccuracies in electrode positioning could impact neuromodulation in the target region, especially in the case of focal montages that employ small electrodes such as HD. Indeed, our simulations suggest an adverse impact on targeting with the 2×2 cm HD electrodes if the overall electrode displacement is more than 2cm from target; with 45.37% and 30.93% decreases in the modal electric field and targeted volume respectively, and a correlation of 0.74 on average.

Another alternative for electrode placement is provided by neuronavigation systems. Indeed, we utilize neuronavigation for the proposed electrode targeting technique, though only during the first visit of the participant. This is an important consideration for clinical trials that include multiple independent tES sessions (24, 25), where using neuronavigation for electrode placement during each visit for each participant (though ideal), could be extremely resource intensive. Before developing the proposed technique, we considered marking the stimulation targets on the scalp using permanent ink post-neuronavigation. However, considering that the ink-marks have to remain present over the course of participation in a clinical trial lasting weeks, and that participants might object to the visible

ink-marks on the scalp, this approach was not pursued. Finally, we also considered using the recently developed Omni-Lateral-Electrode (OLE) system (54). The OLE system is designed specifically for F3/F4 targeting using 5×5cm electrodes, and comes in three sizes (small, medium and large) to account for variations in head size. However, it is not straightforward to extend the OLE system to our cortical brain target, as well as the use of HD-electrode montages.

Validation of the electrode placement technique:

The accuracy of electrode placement was evaluated using neuronavigation data. Measurements revealed an average electrode displacement of 7.0 ± 2.8 mm, which is larger than the 2mm tolerance used in the placement procedure. However, note that the 2mm tolerance is the allowed error at each of the three reference points used in placement, and the larger 7mm error was quantified at visit 6 (i.e. the mid-trial visit) when localizing the stimulation target. The larger 7mm measurement represents an accumulation of error from (a) inaccurate placement of the cap to the aforementioned three reference points, (b) additional error resulting from the non-rigid cap being placed over the head, and (c) potential stretching or wearing out of the cap over time (i.e. by visit 6) with use. Note that no significant differences in positioning accuracy were observed between conventional and HD-tDCS ($p=0.44$), which is expected since determining the scalp location for electrode placement as described in the Electrode placement section does not utilize information about the type of electrode being placed.

To provide context for the observed positioning accuracy, we simulated electric fields induced by conventional and HD-tDCS for three cases of electrode displacements: (a) the observed positioning accuracy (7mm), (b) 1cm, and (c) 2cm (the latter two being half and full length of the smallest electrode dimension). Simulations show that for the observed average displacement of 7mm, the simulated electric fields were highly consistent with the no-displacement case, with a correlation of > 0.90, and <10% change in the modal electric field and targeted volume (Table 2). Overall, the 7mm, 1cm and 2cm electrode displacement cases result in electric field strengths that are similar to the no-electrode-displacement case (with a correlation > 0.80, < 15 % change in the modal electric field, and < 5 % change in the targeted volume), with the exception of 2cm displacements in the HD-montage (wherein an average correlation of 0.58 was observed). Similar results are observed when the metrics are calculated using the electric field normal to the cortical surface. The same pattern of large-scale changes in the 2cm displacement case with the HD-montage is observed when the targeted volume metric is calculated using the following thresholds –(a) 50% of the maximum field amplitude, and (b) the median field-value threshold (see Supplementary S2). Overall, our results are consistent with a recent modeling study that showed that differences of 1 cm in electrode placement result in electric field distributions that have a spatial correlation of 0.8, although the study evaluated correlations using a different montage (19). Note that simulations also show small changes in the electric field for conventional montages with 2cm displacements, which is intuitive considering the large size of the conventional electrodes (5 × 7cm). In contrast, large changes in the electric field distribution were observed for the HD montages, suggesting that the efficacy of targeting in small-sized

electrode employing focal montages such as HD could be significantly impacted with 2cm displacements.

For the 2cm displacement case with the HD montage, simulations predicted a 10–15% reduction in the modal electric field (E-field) on average. If it could be established that some minimum current at the targeted location was sufficient for treatment, and higher currents at that location were known to be safe and therapeutically effective, a relevant question to consider would be whether increasing the applied current intensity to a level sufficient to assure attainment of the required threshold could counteract the average misplacement-induced perturbations in the E-field strength. However, in addition to E-field *strength* within the target region, the effects of stimulation are also dependent on the *spatial distribution* of the E-field. The latter is tracked using the correlation metric shown in Table 2, and in the 2cm case of the HD-montage considered here, the E-field correlation between the displaced and ideal case is 0.58, reflecting large scale changes in the spatial distribution of the E-field. These differences in the spatial distribution of the E-field cannot be rectified by modulating the total applied current, since the latter would only scale the E-field uniformly across all voxels, leaving the spatial pattern unchanged. This pattern is also captured by the correlation metric, which is invariant to scaling effects. Thus, modulating the total applied current will likely not affect outcomes, because while it may help address the reduction in E-field, it cannot address the significant changes in the spatial pattern of the E-field caused by electrode misplacement. Additionally, increasing the applied current amplitude to compensate for misplacement-induced E-field reductions will also increase the E-field in non-target regions, which may lead to stimulation of unintended cortical targets.

Finally, the pCASL data was analyzed and showed significant tDCS-induced increases in %ch-CBF in the active-stimulation group (relative to sham) in the left-DLPFC stimulation-target. These tDCS-induced CBF increases are consistent with prior findings of Zheng et al. and Baeken el al. (49, 50), who also showed CBF increases in response to tDCS. Note that these results are similar to our prior findings demonstrating engagement of the left DLPFC in a mostly overlapping sample (33), where post-treatment CBF-changes had been analyzed after confirming no significant differences in baseline CBF. Notably here, posthoc voxelwise analysis identified the peak significant voxel in this region to be located at $x=-27, y=42, z=19.5$ mm (MNI co-ordinates), which is directly underneath the intended stimulation target at $x=-46, y=44, z=38$ mm (i.e. approximately in the same coronal slice considering the 7.5 mm smoothing threshold, and at an angle of 44.2 degrees in the coronal plane). The *location* of these increases under the stimulation target indicates that the proposed placement technique introduces minimal biases in the spatial location of the cortical coordinate ultimately targeted by tES. These in-vivo findings validate our expectations of accurate targeting (predicted by SIMNIBS simulations), and thus help establish the rigor of the proposed electrode placement technique.

Overall, the placement technique proposed in this work (a) helped control for inter-subject variability by personalizing the stimulation-target to each individual participant, and (b) minimized electrode misplacement at the stimulation-target as estimated through simulations and in-vivo measurements. Critically, the significant CBF increases measured under the stimulation target show that our careful electrode placement technique was successful

in mitigating the combined variability that can result from inter-individual differences in anatomy and electrode misplacement. However, a more detailed comparison of how deviation from the electrode positioning compares to the expected inter-individual variability would be an informative line of inquiry for future research.

Applicability to other brain targets:

Finally, we demonstrate proof of concept that the proposed technique can be used for electrode placement at other scalp targets. Specifically, we chose F2, Fz, F4, F8, Cz, C4, T4, Pz, P4, T6, and O2 MNI coordinates (as reported in (28)) as targets in order to cover most of the scalp. A slightly better accuracy of placement was observed, with the identified sites showing an average displacement of 4.28 ± 2.29 mm from the intended targets (vs. 7.0 ± 2.8 mm measured for the L. DLPFC target). The improved accuracy could be due to the usage of C3, C4 and Cz reference points instead of T7 and T8 (as detailed in the Methods section).

Conclusion:

In this work, we describe a technique that was used to accurately place tES electrodes over a specific cortical stimulation-site in the left DLPFC and across other sites over the rest of the scalp. Taken together, our results show that the proposed electrode placement method can ensure targeting to within 1cm on average. Further, the observed variability in electrode placement results in minimal changes in the electric field distribution on target, as predicted by simulations (> 0.90 correlation, and < 10% changes in the modal electric field and the targeted volume). Finally, our in-vivo observations of increased CBF directly underneath the stimulation target in the active stimulation group relative to sham demonstrates that the proposed electrode placement approach does not introduce appreciable biases in the spatial location ultimately targeted. Note that for specific *cortical* targets such as ours and that are the goal of most clinical trials, existing placement techniques based on *cranial* landmarks (such as the 10–20 EEG system) are not ideal because of (a) systematic bias introduced when approximating the scalp-projection of the cortical target by the closest 10–20 coordinate, and (b) the variance introduced in placement by the imprecise cranio-cortical relationship. Overall, the accumulating inaccuracies in electrode positioning when using the manual 10–20 system could impact neuromodulation in the target region, especially for focal montages such as HD as indicated by our simulations. For this reason, we recommend utilizing the proposed approach for administering tES at cortical targets, especially in clinical trials that investigate focal montages and/or involve repeated tES sessions over multiple days. For translating the proposed electrode placement technique, we recommend piloting placement accuracy in a small sample before the trial starts. This serves to both train staff, and estimate expected electrode displacements, which can be simulated *a priori* to determine the sensitivity of the employed tES montage to electrode displacements. We also recommend measuring electrode displacements in at least one treatment visit per participant in order to confirm the accuracy of electrode placement throughout the trial. Based on this work, the choice of feasible tES stimulation sites can now be extended to include scalp projections of clinically relevant cortical coordinates identified through brain mapping studies, and does not need to be the nearest 10–20 location (which may be suboptimal for spatially precise montages like HD).

Supplementary Material

Refer to Web version on PubMed Central for supplementary material.

Funding:

This research was supported by US NIH grants R61 MH110526 and R01 MH111896.

References:

1. Nitsche MA, Paulus W. Excitability changes induced in the human motor cortex by weak transcranial direct current stimulation. J Physiol. 2000;527 Pt 3:633–9. [PubMed: 10990547]
2. Coffman BA, Clark VP, Parasuraman R. Battery powered thought: enhancement of attention, learning, and memory in healthy adults using transcranial direct current stimulation. NeuroImage. 2014;85 Pt 3:895–908. [PubMed: 23933040]
3. Kuo MF, Chen PS, Nitsche MA. The application of tDCS for the treatment of psychiatric diseases. International review of psychiatry. 2017;29(2):146–67. [PubMed: 28523976]
4. Berryhill ME, Martin D. Cognitive Effects of Transcranial Direct Current Stimulation in Healthy and Clinical Populations: An Overview. The journal of ECT. 2018;34(3):e25–e35. [PubMed: 30095685]
5. Floel A. tDCS-enhanced motor and cognitive function in neurological diseases. NeuroImage. 2014;85 Pt 3:934–47. [PubMed: 23727025]
6. Woods AJ, Antal A, Bikson M, Boggio PS, Brunoni AR, Celnik P, et al. A technical guide to tDCS, and related non-invasive brain stimulation tools. Clinical neurophysiology : official journal of the International Federation of Clinical Neurophysiology. 2016;127(2):1031–48. [PubMed: 26652115]
7. Sanchez-Leon CA, Sanchez-Lopez A, Ammann C, Cordones I, Carretero-Guillen A, Marquez-Ruiz J. Exploring new transcranial electrical stimulation strategies to modulate brain function in animal models. Curr Opin Biomed Eng. 2018;8:7–13. [PubMed: 30272042]
8. Bikson M, Rahman A, Datta A. Computational models of transcranial direct current stimulation. Clinical EEG and neuroscience. 2012;43(3):176–83. [PubMed: 22956646]
9. Hyeon S, Hyoung-Ihl K, Sung Chan J. A computational study on effect of a transcranial channel as a skull/brain interface in the conventional rectangular patch-type transcranial direct current stimulation. Annu Int Conf IEEE Eng Med Biol Soc. 2017;2017:1946–9.
10. Nitsche MA, Fricke K, Henschke U, Schlitterlau A, Liebetanz D, Lang N, et al. Pharmacological modulation of cortical excitability shifts induced by transcranial direct current stimulation in humans. J Physiol. 2003;553(Pt 1):293–301. [PubMed: 12949224]
11. Kuo HI, Bikson M, Datta A, Minhas P, Paulus W, Kuo MF, et al. Comparing cortical plasticity induced by conventional and high-definition 4 × 1 ring tDCS: a neurophysiological study. Brain stimulation. 2013;6(4):644–8. [PubMed: 23149292]
12. Caparelli-Daquer EM, Zimmermann TJ, Mooshagian E, Parra LC, Rice JK, Datta A, et al. A pilot study on effects of 4×1 high-definition tDCS on motor cortex excitability. Annu Int Conf IEEE Eng Med Biol Soc. 2012;2012:735–8.
13. Edwards D, Cortes M, Datta A, Minhas P, Wassermann EM, Bikson M. Physiological and modeling evidence for focal transcranial electrical brain stimulation in humans: a basis for high-definition tDCS. NeuroImage. 2013;74:266–75. [PubMed: 23370061]
14. Mikkonen M, Laakso I, Tanaka S, Hirata A. Cost of focality in TDCS: Interindividual variability in electric fields. Brain stimulation. 2020;13(1):117–24. [PubMed: 31606449]
15. Antonakakis M, Schrader S, Aydin U, Khan A, Gross J, Zervakis M, et al. Inter-Subject Variability of Skull Conductivity and Thickness in Calibrated Realistic Head Models. NeuroImage. 2020;223:117353.
16. Jog MV, Wang DJJ, Narr KL. A review of transcranial direct current stimulation (tDCS) for the individualized treatment of depressive symptoms. Pers Med Psychiatry. 2019;17–18:17–22. [PubMed: 31938757]

17. Fernandez-Corazza M, Turovets S, Luu P, Anderson E, Tucker D. Transcranial Electrical Neuromodulation Based on the Reciprocity Principle. Frontiers in psychiatry. 2016;7:87. [PubMed: 27303311]
18. Huang Y, Thomas C, Datta A, Parra LC. Optimized tDCS for Targeting Multiple Brain Regions: An Integrated Implementation. Annu Int Conf IEEE Eng Med Biol Soc. 2018;2018:3545–8.
19. Opitz A, Yeagle E, Thielscher A, Schroeder C, Mehta AD, Milham MP. On the importance of precise electrode placement for targeted transcranial electric stimulation. NeuroImage. 2018;181:560–7. [PubMed: 30010008]
20. Woods AJ, Bryant V, Sacchetti D, Gervits F, Hamilton R. Effects of Electrode Drift in Transcranial Direct Current Stimulation. Brain stimulation. 2015;8(3):515–9. [PubMed: 25583653]
21. Indahlastari A, Albizu A, Nissim NR, Traeger KR, O'Shea A, Woods AJ. Methods to monitor accurate and consistent electrode placements in conventional transcranial electrical stimulation. Brain stimulation. 2019;12(2):267–74. [PubMed: 30420198]
22. Wiethoff S, Hamada M, Rothwell JC. Variability in response to transcranial direct current stimulation of the motor cortex. Brain stimulation. 2014;7(3):468–75. [PubMed: 24630848]
23. Li LM, Uehara K, Hanakawa T. The contribution of interindividual factors to variability of response in transcranial direct current stimulation studies. Frontiers in cellular neuroscience. 2015;9:181. [PubMed: 26029052]
24. Palm U, Hasan A, Strube W, Padberg F. tDCS for the treatment of depression: a comprehensive review. Eur Arch Psychiatry Clin Neurosci. 2016;266(8):681–94. [PubMed: 26842422]
25. Brunoni AR, Moffa AH, Sampaio-Junior B, Borrione L, Moreno ML, Fernandes RA, et al. Trial of Electrical Direct-Current Therapy versus Escitalopram for Depression. N Engl J Med. 2017;376(26):2523–33. [PubMed: 28657871]
26. Jasper HH. Report of the committee on methods of clinical examination in electroencephalography. Electroencephalography and Clinical Neurophysiology. 1958;10(2):370–5.
27. Silverman D. The Rationale and History of the 10–20 System of the International Federation. American Journal of EEG Technology. 2015;3(1):17–22.
28. Okamoto M, Dan H, Sakamoto K, Takeo K, Shimizu K, Kohno S, et al. Three-dimensional probabilistic anatomical cranio-cerebral correlation via the international 10–20 system oriented for transcranial functional brain mapping. NeuroImage. 2004;21(1):99–111. [PubMed: 14741647]
29. Herwig U, Satrapi P, Schonfeldt-Lecuona C. Using the international 10–20 EEG system for positioning of transcranial magnetic stimulation. Brain Topogr. 2003;16(2):95–9. [PubMed: 14977202]
30. Rich TL, Gillick BT. Electrode Placement in Transcranial Direct Current Stimulation-How Reliable Is the Determination of C3/C4? Brain Sci. 2019;9(3).
31. Sparing R, Buelte D, Meister IG, Paus T, Fink GR. Transcranial magnetic stimulation and the challenge of coil placement: a comparison of conventional and stereotaxic neuronavigational strategies. Hum Brain Mapp. 2008;29(1):82–96. [PubMed: 17318831]
32. University of California LA, National Institute of Mental H. Transcranial Direct Current Stimulation in Major Depression 2022 [updated July 31. Katherine Narr]. Available from: https://ClinicalTrials.gov/show/NCT03556124.
33. Jog MS, Kim E, Anderson C, Kubicki A, Kayathi R, Jann K, et al. In-vivo imaging of targeting and modulation of depression-relevant circuitry by transcranial direct current stimulation: a randomized clinical trial. Transl Psychiatry. 2021;11(1):138. [PubMed: 33627624]
34. Fitzgerald PB, Hoy K, McQueen S, Maller JJ, Herring S, Segrave R, et al. A randomized trial of rTMS targeted with MRI based neuro-navigation in treatment-resistant depression. Neuropsychopharmacology. 2009;34(5):1255–62. [PubMed: 19145228]
35. Rajkowska G, Goldman-Rakic PS. Cytoarchitectonic definition of prefrontal areas in the normal human cortex: II. Variability in locations of areas 9 and 46 and relationship to the Talairach Coordinate System. Cereb Cortex. 1995;5(4):323–37. [PubMed: 7580125]
36. Koessler L, Maillard L, Benhadid A, Vignal JP, Felblinger J, Vespignani H, et al. Automated cortical projection of EEG sensors: anatomical correlation via the international 10–10 system. NeuroImage. 2009;46(1):64–72. [PubMed: 19233295]

37. Harms MP, Somerville LH, Ances BM, Andersson J, Barch DM, Bastiani M, et al. Extending the Human Connectome Project across ages: Imaging protocols for the Lifespan Development and Aging projects. NeuroImage. 2018;183:972–84. [PubMed: 30261308]
38. Kilroy E, Apostolova L, Liu C, Yan L, Ringman J, Wang DJ. Reliability of two-dimensional and three-dimensional pseudo-continuous arterial spin labeling perfusion MRI in elderly populations: comparison with 15O-water positron emission tomography. J Magn Reson Imaging. 2014;39(4):931–9. [PubMed: 24038544]
39. Brainbox-Neuro. Brainsight Neuronavigation [Available from: https://brainbox-neuro.com/catalogue/neuro-navigation/tms-navigation/brainsight-tms-navigation/.
40. BrainProducts. EASYCAP GmbH [Available from: https://www.brainproducts.com/productdetails.php?id=20.
41. Penny WD, Ashburner J, Kiebel S, Henson R, Glaser DE, Phillips C, et al. Statistical parametric mapping: An annotated bibliography. 2001 [Available from: http://www.fil.ion.ucl.ac.uk/spm/bib.htm.
42. Smith SM, Jenkinson M, Woolrich MW, Beckmann CF, Behrens TE, Johansen-Berg H, et al. Advances in functional and structural MR image analysis and implementation as FSL. NeuroImage. 2004;23 Suppl 1:S208–19. [PubMed: 15501092]
43. Thielscher A, Antunes A, Saturnino GB. Field modeling for transcranial magnetic stimulation: A useful tool to understand the physiological effects of TMS? Annu Int Conf IEEE Eng Med Biol Soc. 2015;2015:222–5.
44. Wagner S, Rampersad SM, Aydin U, Vorwerk J, Oostendorp TF, Neuling T, et al. Investigation of tDCS volume conduction effects in a highly realistic head model. J Neural Eng. 2014;11(1):016002.
45. Opitz A, Paulus W, Will S, Antunes A, Thielscher A. Determinants of the electric field during transcranial direct current stimulation. NeuroImage. 2015;109:140–50. [PubMed: 25613437]
46. Freedman D, Diaconis P. On the histogram as a density estimator:L 2 theory. Zeitschrift für Wahrscheinlichkeitstheorie und Verwandte Gebiete. 1981;57(4):453–76.
47. MathWorks, MATLAB. Histogram bin counts [Available from: https://www.mathworks.com/help/matlab/ref/histcounts.html.
48. Alsop DC, Detre JA, Golay X, Gunther M, Hendrikse J, Hernandez-Garcia L, et al. Recommended implementation of arterial spin-labeled perfusion MRI for clinical applications: A consensus of the ISMRM perfusion study group and the European consortium for ASL in dementia. Magn Reson Med. 2015;73(1):102–16. [PubMed: 24715426]
49. Zheng X, Alsop DC, Schlaug G. Effects of transcranial direct current stimulation (tDCS) on human regional cerebral blood flow. NeuroImage. 2011;58(1):26–33. [PubMed: 21703350]
50. Baeken C, Remue J, Vanderhasselt MA, Brunoni AR, De Witte S, Duprat R, et al. Increased left prefrontal brain perfusion after MRI compatible tDCS attenuates momentary ruminative self-referential thoughts. Brain stimulation. 2017;10(6):1088–95. [PubMed: 28917591]
51. Sallet J, Mars RB, Noonan MP, Neubert FX, Jbabdi S, O'Reilly JX, et al. The organization of dorsal frontal cortex in humans and macaques. J Neurosci. 2013;33(30):12255–74. [PubMed: 23884933]
52. Fox MD, Buckner RL, Liu H, Chakravarty MM, Lozano AM, Pascual-Leone A. Resting-state networks link invasive and noninvasive brain stimulation across diverse psychiatric and neurological diseases. Proceedings of the National Academy of Sciences of the United States of America. 2014;111(41):E4367–75. [PubMed: 25267639]
53. Clark VP, Coffman BA, Mayer AR, Weisend MP, Lane TD, Calhoun VD, et al. TDCS guided using fMRI significantly accelerates learning to identify concealed objects. NeuroImage. 2012;59(1):117–28. [PubMed: 21094258]
54. Seibt O, Brunoni AR, Huang Y, Bikson M. The Pursuit of DLPFC: Non-neuronavigated Methods to Target the Left Dorsolateral Pre-frontal Cortex With Symmetric Bicephalic Transcranial Direct Current Stimulation (tDCS). Brain stimulation. 2015;8(3):590–602. [PubMed: 25862601]

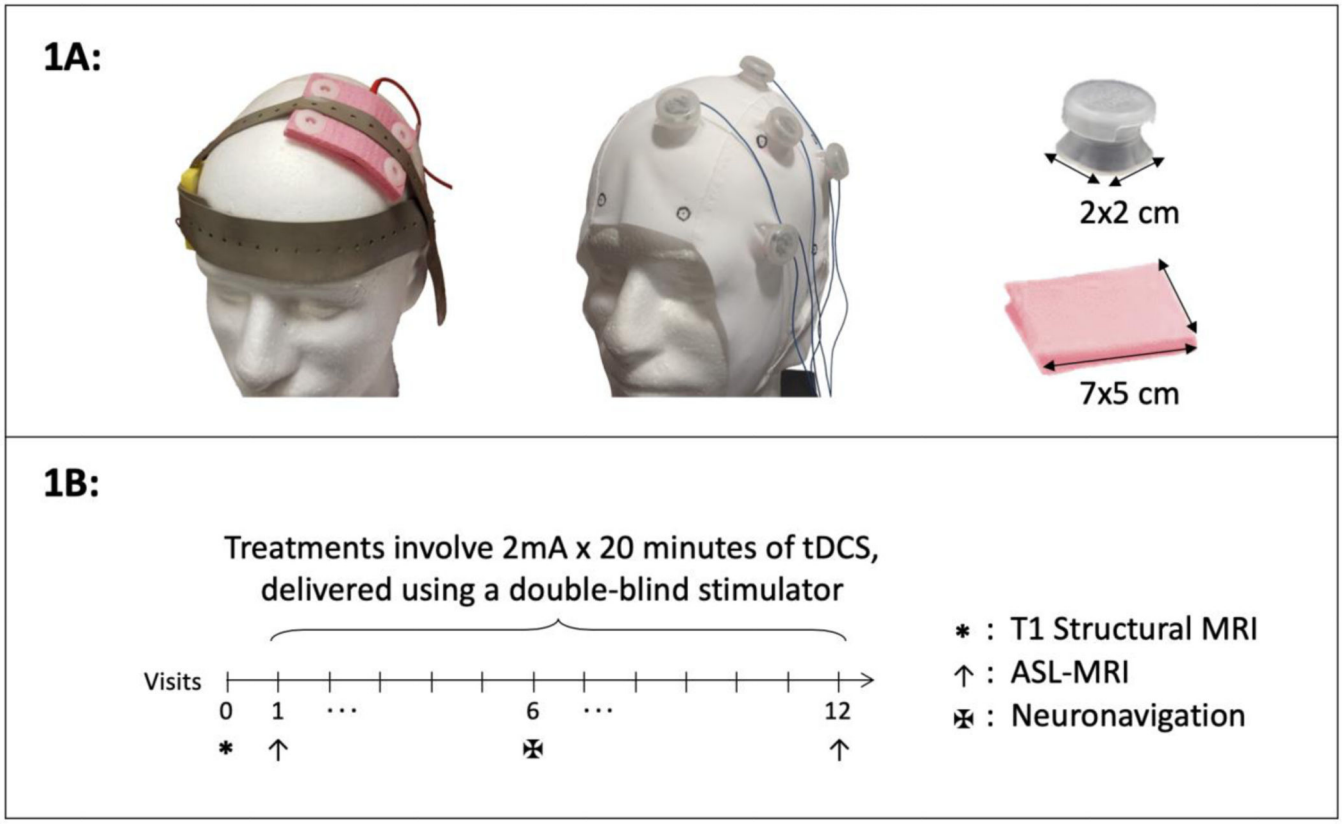

Figure 1: Montages and study design.

1A shows the montages employed. The stimulation target was chosen to be the scalp projection (individualized to each participant) of *x=−46, y=44, z=38* mm (MNI coordinates). For the high-definition (HD) montage, 2×2 cm sized electrodes were used in a 4×1 ring montage, with the anode positioned on the stimulation target, and the cathodes placed 5cm away from the anode, and equidistant from the two neighboring cathode electrodes. For the Conventional montage, 5×7 cm sponge electrodes were used with the anode positioned on the stimulation target and the cathode placed over *x=56, y=30, z=−1* (MNI coordinates), approximating the F8 location. **1B** shows the acquisition of study-relevant data over the course of the study for each participant, with (i) T1 structural data acquired at visit 0, (ii) neuronavigation data acquired at mid-trial (visit 6), and (iii) cerebral blood flow (CBF) data acquired using arterial spin labeling (ASL) MRI at baseline and post-treatment (visits 1 and 12). Note that neuronavigation was used at baseline to locate and mark the individualized stimulation-target on the participant's cap (as described in Methods, Electrode Placement section). Any observed displacements at this initial visit were corrected to ensure accurate localization of the stimulation-target for subsequent treatments.

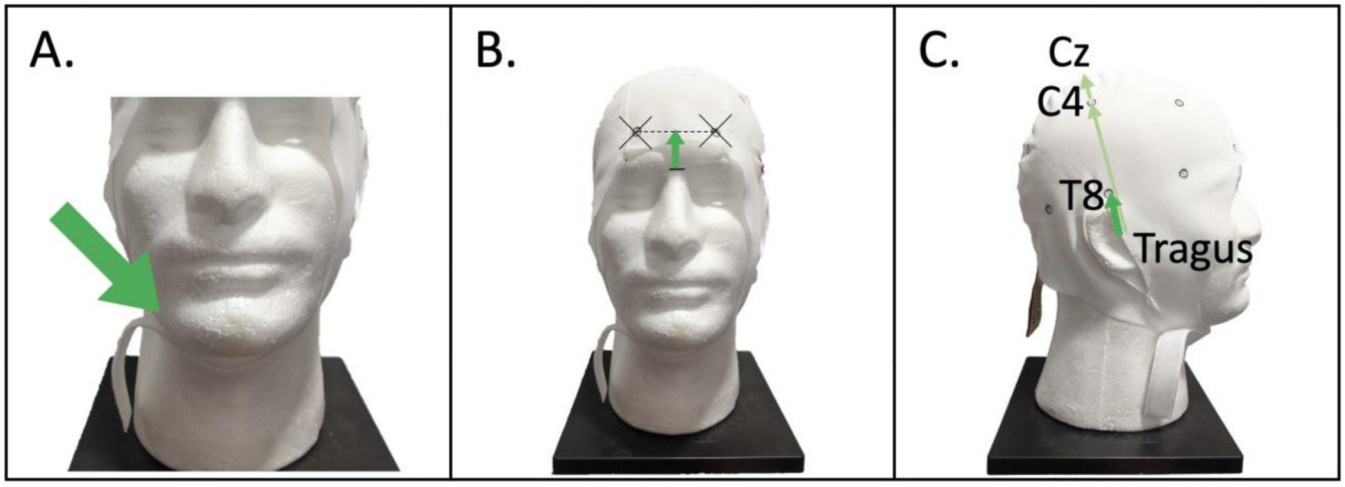

Figure 2: Cap Placement technique.

EEG caps are individually fit to each participant as follows: The cap is first secured using a chin strap, and the position of the strap is marked so that it can be secured with the same tension at follow-up sessions (**2.A**, green arrow). Next, the nasion to inion distance is measured, and the cap is adjusted such that the midpoint of the line joining Fp1 and Fp2 is 10% of the nasion-to-inion distance (**2.B).** Following this, the cap is adjusted to ensure that the T7 and T8 reference points are at identical distances from the left and right tragus (**2.C**). Finally, the cap is secured by taping it down over the participant's upper cheeks and between the eyebrows. The nasion to Fp1/Fp2 distance, along with the tragus to T7/T8 distances are recorded. For all subsequent sessions with the same participant, the cap is placed to match these distances to within 0.2cm. When investigating the accuracy of the proposed technique for other brain targets, piloting indicated that using the left tragus to C3, right tragus to C4, and left/right tragus to Cz provided slightly better accuracy than the T7/T8 reference points. Consequently, these reference points were utilized instead of T7 and T8 (shown in **2.C**, light-green arrows). Note that the exact correspondence of the reference points on the cap to the actual T7, T8 etc. is not important, what is crucial for correct cap-placement is to ensure that the distances of the reference points to anatomical landmarks are within the 0.2 cm tolerance.

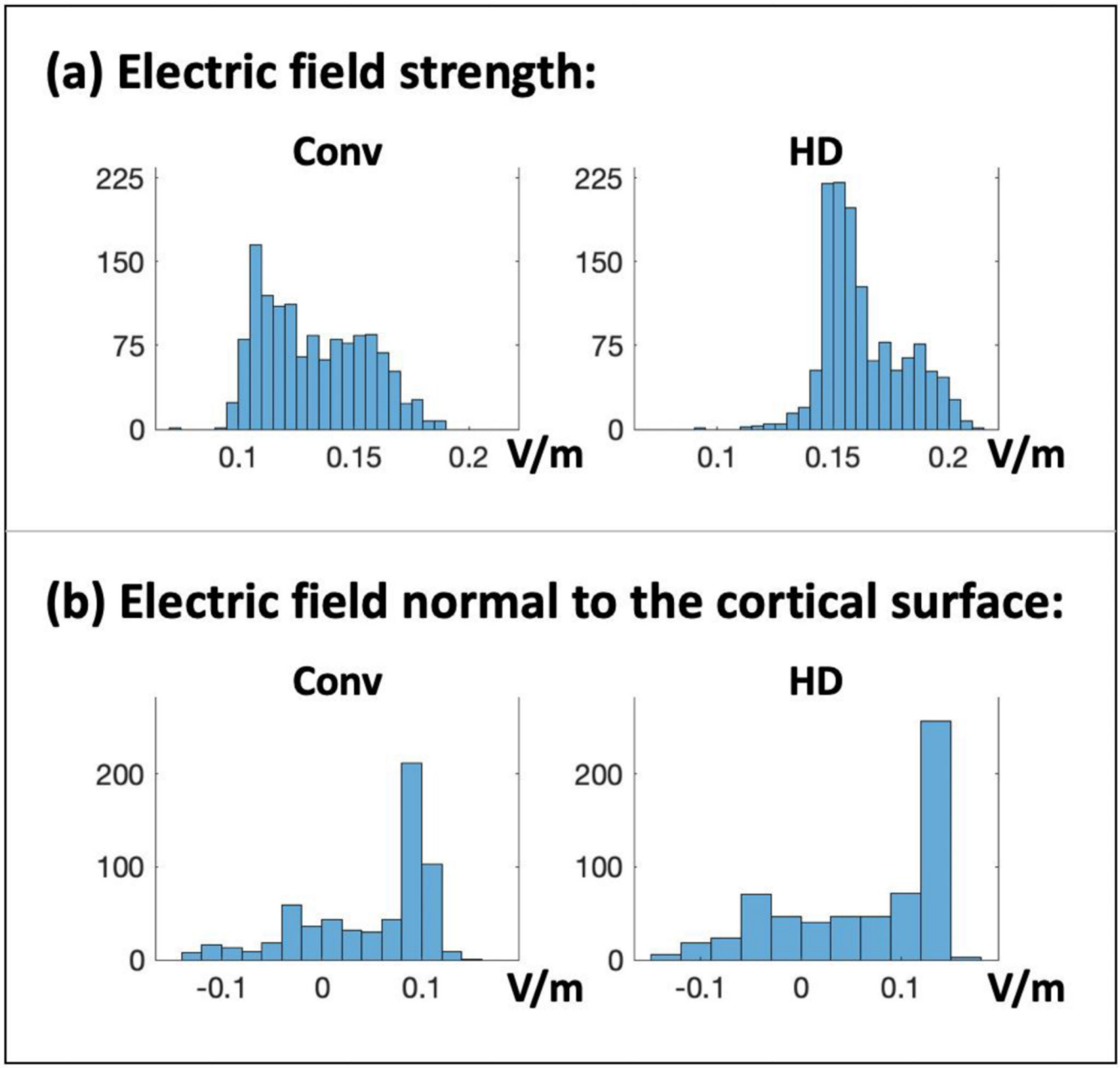

Figure 3: Distribution of the electric field at zero displacement.

Figure shows the distribution of the (a) the electric field (E-field) strength, and (b) electric field normal to the cortical surface, in the 1cm spherical ROI centered at the stimulation target in the ideal zero-displacement case for both the conventional and high-definition tES montages. In all cases, the distribution was observed to be heavy-tailed, providing motivation for the use of the modal electric field as a summary statistic rather than the mean. The modal electric field was calculated after data-binning using the Freedman-Diaconis (41) criterion for heavy-tailed distributions

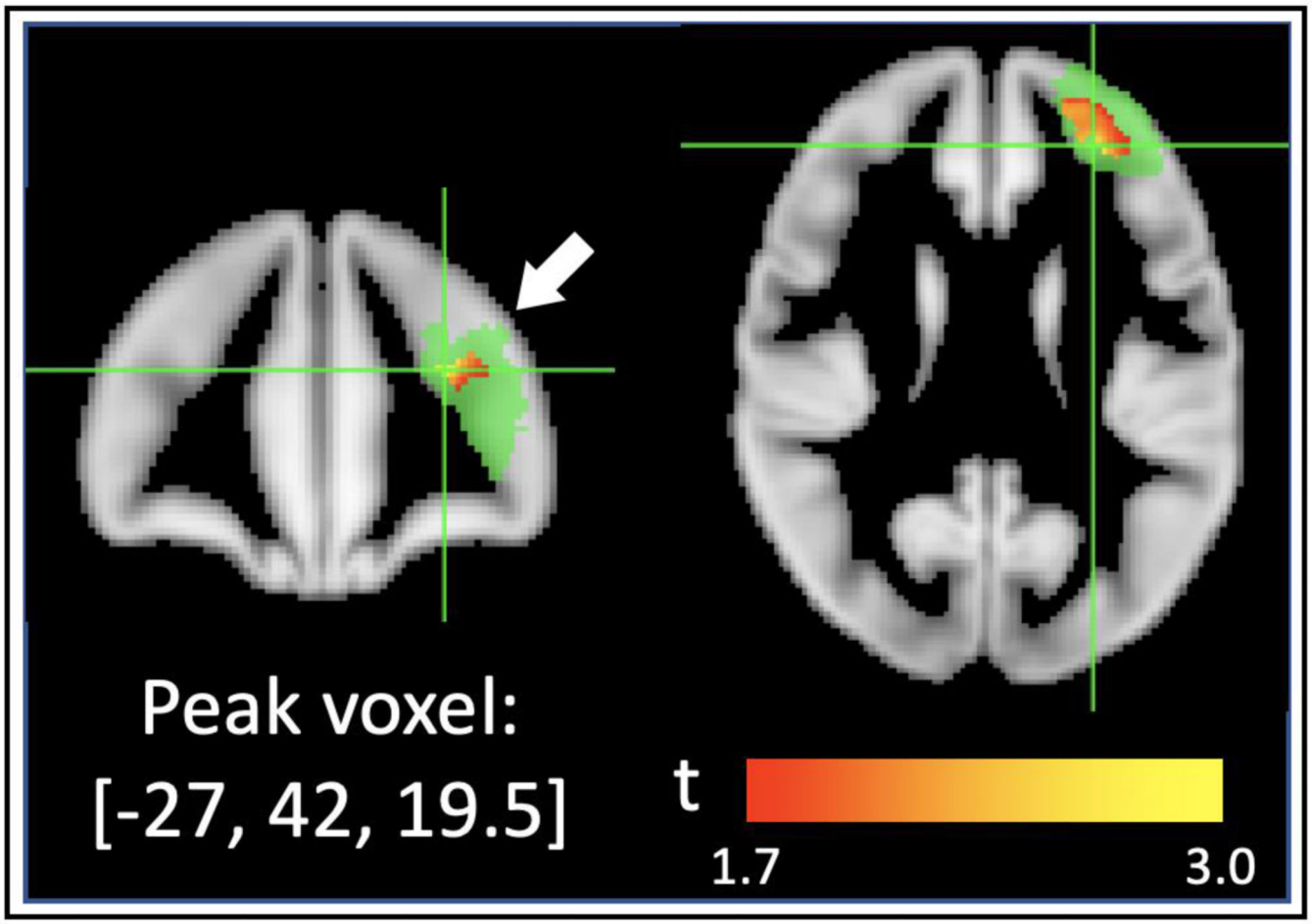

Figure 4: CBF increases near the stimulation target.

A significant increase in the percentage-change cerebral blood flow (%ch-CBF, post-treatment relative to baseline) was observed in the active stimulation group relative to sham in the left DLPFC ($p = 0.046$). The left DLPFC region was defined using an anatomical ROI from the Sallet atlas (51), and is shown in green. Within this region, the peak significant voxel was observed to be at *x=−27, y=42, z=19.5* mm (MNI co-ordinates), and was located using posthoc t-tests that were performed voxel-wise ($p < 0.05$, and shown with the red-yellow colormap). For comparison, the cortical stimulation target is shown with a white arrow. Note that the stimulation target was located at *x=−46, y=44, z=38* mm, which is approximately in the same coronal slice (within the 7.5 mm smoothing threshold) at an angle of 44.2 degrees in the coronal plane.

Table 1.

Accuracy of electrode placement.

Distances between the intended stimulation site and the actual stimulation site (the latter identified using the cap-placement technique) were measured using the Brainsight neuronavigation system at the mid-trial visit (visit #6). Overall, the electrodes were off by 7.0 ± 2.8 mm on average, with a maximum displacement of 13 mm. No significant differences were observed between the HD and Conv groups ($p = 0.44$, two sample t-test), with each group showing a mean displacement of 6.7 ± 2.7 mm and 7.3 ± 3.0 mm respectively.

	Total	HD	Conv
Mean (mm)	7.0	6.7	7.3
SD (mm)	2.8	2.7	3.0
Max (mm)	13	11	13
N (#)	48	23	25

Table 2:

Simulations comparing electric fields induced by displaced electrodes to the ideal zero-displacement case.

2A shows (electric) field strengths in displaced montages, compared to the ideal case. Three displacement scenarios were considered (a) 7mm (the experimentally observed electrode displacements on average), (b) 10mm, and (c) 20mm; with the latter two being half, and full lengths of the smallest electrode dimension (Fig 1). For (a), electric fields were observed to be highly consistent with the no-displacement case, with a correlation of > 0.90, and <10% change in the modal electric field and targeted volume. For (b) and (c), with the exception of the 20mm displacement case with the HD montage, electric field strengths in the displaced montages were also observed to be similar to the ideal zero-displacement montage, with an average Pearson correlation > 0.80, and a < 15% change in the modal electric field and targeted volume. Similar results were observed when the analysis was performed using the electric fields normal to the cortical surface (shown in **2B**). In contrast, 20mm displacements in the HD montage showed large changes, with an average Pearson correlation coefficient of 0.58 for the electric field strength. Although the correlation improved in this case when only electric fields normal to the cortical surface were considered (r = 0.74), large changes were observed in the modal electric field and targeted volume (−45.37% and −30.93% respectively), indicating a significant impact of 20mm displacements on the HD-montage.

A. Changes in Electric field strength with electrode displacement

		(Montage)	Electrode Displacements		
			7mm	10mm	20mm
Pearson r		Conv	0.99	0.98	0.92
		HD	0.91	0.86	0.58
%change	modal E-field	Conv	3.49	4.65	11.63
		HD	−2.13	−0.49	−3.28
	targeted volume	Conv	0.00	0	0.00
		HD	0.00	0	−0.02

B. Changes in electric fields normal to the cortical surface with electrode displacement

		(Montage)	Electrode Displacements		
			7mm	10mm	20mm
Pearson r		Conv	0.99	0.99	0.96
		HD	0.96	0.94	0.74
%change	modal E-field	Conv	4.17	8.33	−8.33
		HD	−5.56	−9.26	−45.37
	targeted volume	Conv	−0.32	0.32	−0.19
		HD	−2.09	−3.64	−30.93

Table 3.

Accuracy of the proposed technique at targets over the rest of the scalp.

MNI coordinates of F2, Fz, F4, F8, Cz, C4, T4, Pz, P4, T6, and O2 (reported in (28)) were chosen as targets to ensure reasonable coverage of the full scalp. Displacements from these targets was measured using Brainsight in a small sample (4 participants X 2 raters) to provide proof of concept that the developed electrode placement technique is applicable to targets over the rest of the scalp. Overall, an average displacement of 4.28 ± 2.29 mm was observed, with a maximum displacement of 12.79 mm.

Target	Mean (mm)	SD(mm)	Max(mm)
F2	4.22	2.10	7.47
Fz	3.23	2.48	7.42
F4	3.62	1.93	7.22
F8	3.50	1.27	5.16
Cz	5.25	3.46	10.49
C4	3.63	1.70	5.81
T4	3.88	1.35	5.46
Pz	5.39	3.79	12.79
P4	4.76	2.02	7.82
T6	4.24	1.80	7.12
O2	5.37	2.30	8.60
Overall	4.28	2.29	12.79